



**HAL**  
open science

## Vessel extraction in coronary X-ray Angiography.

Yuan Wang, Christine Toumoulin, Huazhong Shu, Zhendong Zhou,  
Jean-Louis Coatrieux

► **To cite this version:**

Yuan Wang, Christine Toumoulin, Huazhong Shu, Zhendong Zhou, Jean-Louis Coatrieux. Vessel extraction in coronary X-ray Angiography.. Conference proceedings : .. Annual International Conference of the IEEE Engineering in Medicine and Biology Society. IEEE Engineering in Medicine and Biology Society. Annual Conference, Institute of Electrical and Electronics Engineers (IEEE), 2005, 2, pp.1584-7. 10.1109/IEMBS.2005.1616739 . inserm-00363628

**HAL Id: inserm-00363628**

**<https://www.hal.inserm.fr/inserm-00363628>**

Submitted on 23 Feb 2009

**HAL** is a multi-disciplinary open access archive for the deposit and dissemination of scientific research documents, whether they are published or not. The documents may come from teaching and research institutions in France or abroad, or from public or private research centers.

L'archive ouverte pluridisciplinaire **HAL**, est destinée au dépôt et à la diffusion de documents scientifiques de niveau recherche, publiés ou non, émanant des établissements d'enseignement et de recherche français ou étrangers, des laboratoires publics ou privés.

# Vessel extraction in coronary X-ray Angiography

Y. Wang<sup>1</sup>, C. Toumoulin<sup>2</sup>, H. Z. Shu<sup>1</sup>, Z. D. Zhou<sup>1</sup> and J. L. Coatrieux<sup>2</sup>

<sup>1</sup>Laboratory of Image Science and Technology, Southeast University, Nanjing, P.R.China

<sup>2</sup>Laboratoire Traitement du Signal et de l'Image,INSERM-Université de Rennes I, Rennes, France

**Abstract**—This paper describes a method to extract the vascular centerlines and contours in coronary angiography. The proposed approach associates geometric moments for the estimation of a "cylinder-like model" and relies on a tracking process. The orientation of the cylinder axis and its local diameter are computed from the analytical expressions of the geometric moments of up to order 2. Experimental results are presented on several images of two sequences that show the efficiency of the method.

**Index Terms**—coronary angiography, centerlines and contours extraction, 2D geometric moments, structure tracking

## I. INTRODUCTION

Coronary network reconstruction from X-ray biplane angiography, has motivated a lot of research both for diagnosis and therapeutic purposes [1][2][3][4]. The objective is to reach a quantitative description of coronary geometry and motion, which are required to evaluate the degree of severity of pathology or in the frame of a catheter-based interventional procedure, to help the guidance of the catheter and follow the revisualization process. Because structures are displayed in a 2D format, geometric features and curvature dynamic variations of these structures are difficult to handle. Therefore the 3D coronary reconstruction, which is performed from two views, has to rely on preliminary segmentation, branch formation and matching stages.

This paper is focused on the edge lines and centerlines extraction of the coronary tree. Many methods have been developed to extract these features [5] [6] [7]. But the complex appearances of these structures in the image frame (high curvatures, loops, superpositions, crossings of vessels, and so on) make this detection difficult. This explains why several works have used an interactive mode for the selection of sensitive points for active contour control [1] or for a rough piecewise approximation of the segments followed by a dynamic programming path search [3]. The proposed method is fully automatic and relies on the 2-D geometric moments and the vessel modeling by a cylinder to extract its central axis and local diameters (section II). Section III briefly describes the tracking process. Preliminary results are then presented in section IV, on several angiographic images. Section V concludes on the interest of the method and gives some perspectives.

This work is supported by both the National Natural Science Foundation of China (Grant No.60272045) and the program for New Century Excellent Talents in University.

## II. LOCAL SHAPE MODELING AND GEOMETRIC MOMENTS

Moments are integral-based features and are therefore robust against noise. Furthermore low order moments have a direct geometric interpretation. Their application provides consequently an efficient way to compute location, orientation and size features of elongated bright structures.

### A. Local vessel modeling

The vessel was locally modeled by a cylinder of orientation  $\theta$  and diameter  $d$  (Fig. 1). In the Cartesian coordinate system (E1),  $\theta$  represented the angle between the axis of the cylinder and the Ox axis. The vessel intensity was denoted  $I_v$  and the background intensity  $I_b$ , with  $I_v > I_b$ .

### B. Feature extraction and Geometric moments

The  $(p + q)^{th}$  order of geometric moments applied on an  $N_x \times N_y$  square window, for an image function,  $f(x, y)$  is defined as [8]:

$$m_{pq} = \sum_{p=1}^{N_x} \sum_{q=1}^{N_y} x^p y^q f(x, y) \quad \text{with } p, q \in \mathbb{Z}^+ \quad (1)$$

Furthermore, the  $(p + q)^{th}$  central geometric moment is defined so as to normalize moment calculation with respect to the image centroid, thus yielding moments invariant to object translation:

$$\mu_{pq} = \sum_p \sum_q (x - \bar{x})^p (y - \bar{y})^q f(x, y) \quad (2)$$

where  $(\bar{x}, \bar{y})$  represents the coordinates of the local centroid inside the square window:

$$\bar{x} = \frac{m_{1,0}}{m_{0,0}} \quad \text{and} \quad \bar{y} = \frac{m_{0,1}}{m_{0,0}} \quad (3)$$

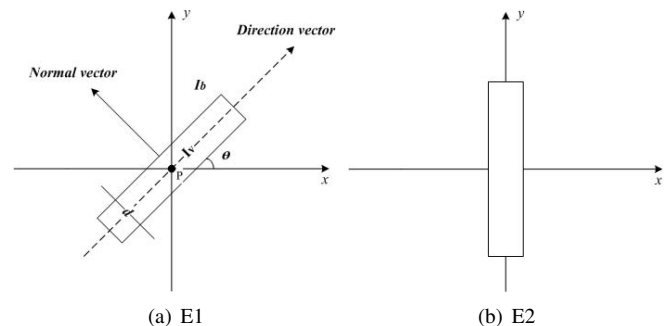


Fig. 1. Vessel modeling: (a) initial coordinate system (E1); (b) coordinate system after alignment on the y axis (E2)

Central moments were applied on an isotropic grid using a circular window. Each pixel inside this window was weighted according to its membership of the circle, by considering a sub-pixel decomposition (Fig. 2). The moment computation was therefore reduced to mask convolutions:

$$\mu_{pq} = f(x, y) * w_{pq}(x, y) \quad (4)$$

where  $w_{pq}$  represents the moment filter mask of order  $(p, q)$ :

$$w_{pq}(x, y) = (x - \bar{x})^p (y - \bar{y})^q A(x, y) \quad (5)$$

The distance between the window center and its gravity center allows to detect whether the window is centered on a bright structure or not. Therefore the central moments can be expressed in terms of moments  $m_{p,q}$  and this gravity center:

$$\begin{aligned} \mu_{2,0} &= m_{2,0} - m_{0,0}\bar{x}^2 \\ \mu_{0,2} &= m_{0,2} - m_{0,0}\bar{y}^2 \\ \mu_{1,1} &= m_{1,1} - m_{0,0}\bar{x}\bar{y} \end{aligned} \quad (6)$$

The local orientation of the structure is given by these three central moments of the second order. In our case, the vessel, being mapped onto an ellipsoid centered at  $(x_0, y_0)$ , the orientation angle with respect to the  $x$ -axis is given by [9]:

$$\theta = \frac{1}{2} \arctan \left( \frac{2\mu_{1,1}}{\mu_{2,0} - \mu_{0,2}} \right) \quad (7)$$

The local vessel diameter is then expressed in terms of the zero order moment and the vessel and background intensities:

$$d = 2 \left[ \frac{m_{0,0} - I_b \pi R^2}{\pi(I_v - I_b)} \right]^{1/2} \quad (8)$$

### III. TRACKING PROCESS

The initialization of the tracking was performed from a list of seed points, automatically extracted at a preliminary stage. From one seed point  $P_i$ , its position was first refined through an iterative process to make it converge towards the central axis. Then the local diameter was estimated using a multi-scale local moment computation to take into account

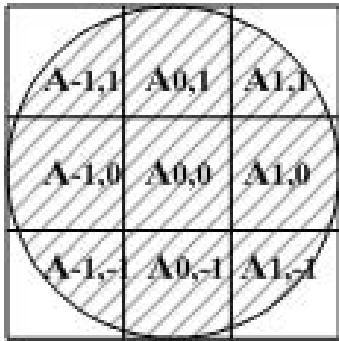


Fig. 2. 2-D Moment mask: Sub-pixel decomposition and weights  $A_{i,j}$  associated to each pixel for a circular window of radius  $R = 1$  (defined in a square window of size  $N = 3$ )

the size variation of the vessel in presence of pathology (stenosis, aneurysm). Afterwards the tracking process was carried out by shifting a circular window towards the next point  $P_{i+1}$  according to the estimated direction at point  $P_i$ . The incremental displacement between these two points was made adaptive and depended on the vessel size and curvature [9][10].

#### A. Estimation of the $P_{i+1}$ Position

The position  $P_{i+1}$  inside the cylinder corresponded to the center of gravity in the circular window. Nevertheless, the orientation estimated at a given position of the window does not guarantee a precise positioning at the next point along the vessel in particular when highly curved vessels are tracked. An iterative centering was therefore performed based on the first order moments to move the point towards the vessel center (Fig.3). It consisted in:

1. Computing the gravity center inside the window,
2. Moving the center of the window to its gravity center
3. Reiterating step 1 and 2 till the center of the window coincides with its gravity center.

#### B. Estimation of the vessel and background intensities

The intensities inside ( $I_v$ ) and outside ( $I_b$ ) the vessel were made adaptive at each step of the tracking to take into account the heterogeneity of the intravascular and environmental properties. The background intensity  $I_b$  was set to the mean value computed outside the vessel in its normal direction. In the same way, the vessel intensity  $I_v$  was equal to the mean intensity computed along the estimated vessel direction.

#### C. Multi-scale detection strategy

The size of the vessels can widely vary (from 25 to a very few pixels) when considering the overall coronary tree or when diseases are concerned (stenosis, aneurysm). In addition, the analytical diameter formulation as reported in (8) depends directly on the window size as well as

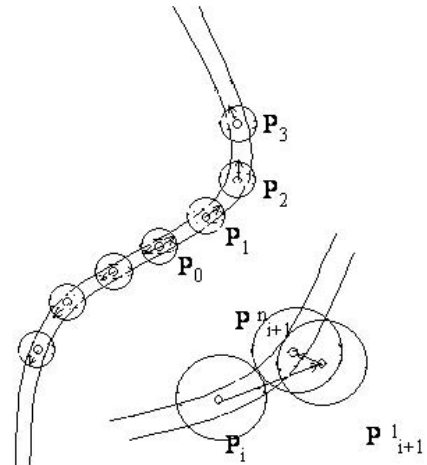


Fig. 3. Tracking process and iterative centering of the point  $P_{i+1}$

the precision of the localization of the vessel center  $P_i$ . Indeed, the vessel corresponds to brighter structures in the image. Therefore optimal parameters are achieved when the spherical window is centered on the vessel axis and its size exactly fits the vessel size. We made this window size adaptive to adjust it, at each step of the tracking, according to the estimated diameter of the vessel. Considering  $R_{i-1}$ , the local estimated radius of the vessel at point  $P_{i-1}$ , the local diameter computation at point  $P_i$ , was performed at different scales according to the following algorithm:

Algorithm **Multi-scale diameter computation**

$$R_{i,n=1} = R_{i-1}$$

Repeat

- 1 Estimate  $P_i, \theta_i, d_i, I_b, I_v$
- 2 If  $(R_{i,n} < d_i/2)$   $R_{i,n+1} = R_{i,n} + 1$   
 Else if  $(R_{i,n} + 1.25 > d_i/2)$   $R_{i,n+1} = R_{i,n} - 1$   
 Else  $R_{i,n+1} = R_{i,n}$
- 3  $n = n + 1$ ;

while  $(R_{i,n} \neq R_{i,n-1})$

End

The local direction  $\theta_i$  was computed on a window centered at point  $P_i$  and with radius  $(R_{i,n} + 1)$ .

D. Re-initialization procedure

The tracking can be stopped when meeting high curvature or superposition of vessels. A square box, twice the size of the computation window, centered on the last extracted point  $P_i$ , was then open and an intersection of vessels with the perimeter of the window was searched. The previously visited pixels were marked in order to avoid a potential backtrack.

E. End Conditions

The stopping conditions, checked at each step, allow testing the location of the estimated point (inside/outside). This decision relies on the mean intensity and standard deviation values estimated within the current tracking window compared to a reference corresponding to a minimal diameter vessel  $d_{min}$  that can be detected. In any case, the vessel intensity must be higher than the background one ( $I_v > I_b$ ).

F. Branch formation

The tracking allowed to extract points located on the central axis of the vessel and to estimate the local diameter at each of these points. The objective was then to establish the continuity between these points (centerlines and edge lines respectively) in order to reconstitute the vascular branches. Centerlines were first reconstituted based on intensity and directional similarity criteria.

A branch was delimited by a bifurcation point or a end point. Then for each centerline, edge points were recovered in the normal direction to the vessel. The spatial location of each point, related to the central axis, was used to construct the left and right contours (Fig. 4). At each bifurcation point, a circle was drawn whose radius was equal to the largest

diameter among the estimated radii in the neighborhood of the bifurcation at each starting centerline. Then, edge points were picked up at the level of the intersection of each centerline with the circle. The continuity was then obtained by simply connecting the edge points, located in the same side related to the central axis.

IV. RESULTS

The algorithm was applied on angiographic subtracted images ( $512 \times 512$ , 8 bits) acquired in standard conditions (Left and Right Anterior Oblique views) with a General Electric Digital Subtraction Angiography system (Fig 5). Each sequence includes 15 images. The images were first convolved with a Gaussian filter of size  $9 \times 9$  and standard deviation equal to 0.5 to smooth the noise. A morphological top hat operator was then applied with a spherical structuring element of size  $41 \times 41$  to enhance the structure of interest. Four horizontal lines were then drawn on each image and points corresponding to maximum intensity points, were extracted on each line. These points were normally located on the crest line of the main vascular branches. They were kept as initial seed point to initialize the tracking process.

The tracking process was applied on each image of each sequence. For illustration, extracted centerlines and contours are shown in Fig.6 and Fig.7 for two images of each sequence. Results are superposed on the original images

V. CONCLUSION

The tracking process allows extracting the centerlines and contours of the main vascular branches within 10 seconds per image on a Pentium-4 PC with 1.5 GHz CPU and 512 Mb RAM. Results show a good efficiency of the method on the set of the images of each sequence. Some refinements are nevertheless necessary to obtain more accurate and smooth contours. The next stages will be devoted to the evaluation of the algorithm to other angiographic sequences: (1) its robustness with regard to the presence of other possible conformations in the images and (2) the accuracy of the detection.

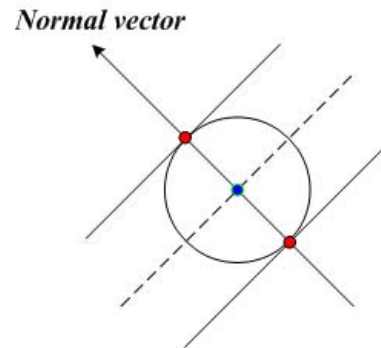


Fig. 4. Edge point recovering: for each extracted central axis point (blue point), contour points are got from the local estimated diameter in the normal direction to the vessel (red points).

## REFERENCES

- [1] S-Y. J. Chen and J. D. Carroll, "Kinematic and Deformation Analysis of 4D Coronary Arterial Trees Reconstructed from Cine Angiograms," *IEEE Trans. Med. Imag.*, vol. 22, no. 6, pp. 724–740, 2003.
- [2] J-L. Coatrieux, M. Garreau, R. Collorec and C. Roux, "Computer Vision Approaches for the Three Dimensional Reconstruction of Coronary Arteries: Review and Prospects," *Critical Reviews in Biomedical Engineering*, vol. 22, no. 1, pp. 1–38, 1994.
- [3] F. Mourgues, F. Devernay, G. Malandain and E. Coste-Manire. "3D+T modeling of coronary artery tree from standard non-simultaneous angiograms," *In Proc. MICCAI*, vol. 2208, pp. 1320-1322, 2001.
- [4] A. Sarwal and A. P. Dhawan, "Three-dimensional reconstruction of coronary arteries from two views," *Computer methods and programs in Biomedicine*, vol. 65, pp. 25–43, 2001.
- [5] C. Toumoulin, R. Collorec, J. L. Coatrieux, "Vascular network segmentation in subtraction angiograms," *a comparative study*, *Medical Informatics*, vol. 15 no. 4, pp. 333–341, 1990.
- [6] Y. Sun, "Automated identification of vessel contours in coronary arteriograms by an adaptive tracking algorithm," *IEEE Transactions on Medical Imaging*, vol. 8, no. 1, pp. 78–88, 1989.
- [7] J. L. Coatrieux and C. Toumoulin, "Computational vision and structural modeling in cardiac vascular network reconstruction," *Medical Imaging Processing: from pixel to structure*, Edited by Yves Goussard, Editions de l'école polytechnique de Montreal, pp. 83–109, 1998.
- [8] M. Shling, et al. "Multiresolution moment filters: Theory and applications," *in Proc. IEEE. Transactions on Image Processing*, vol. 13, no. 4, pp. 483–495, 2004.
- [9] C. Boldak, Y. Rolland, C. Toumoulin and J. L. Coatrieux J.L., *Journal of Biocybernetics and Biomedical Engineering*, vol. 3 no. 1, pp. 41–64, 2003.
- [10] P. Reuzé, et al, *Journal of Technology and Health Care I*, pp. 181–188, 1993.

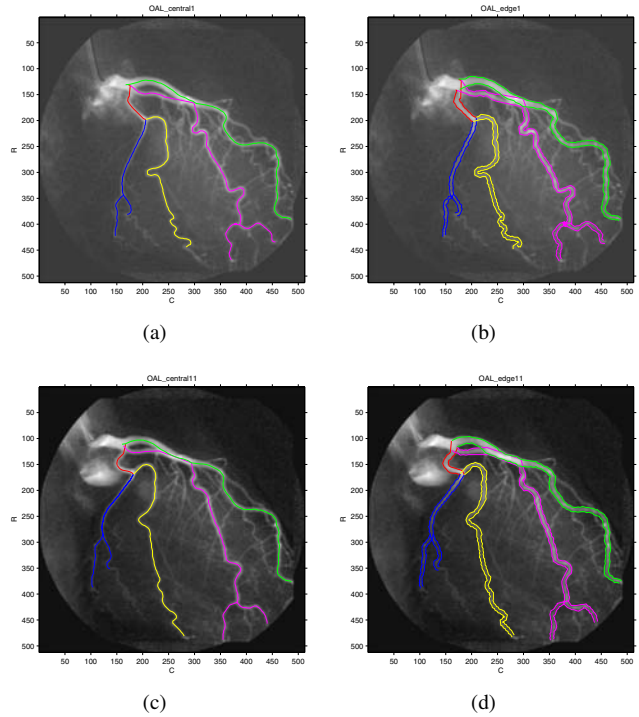


Fig. 6. Extracted centerlines and contours for images 1 and 11 of the LAO sequence

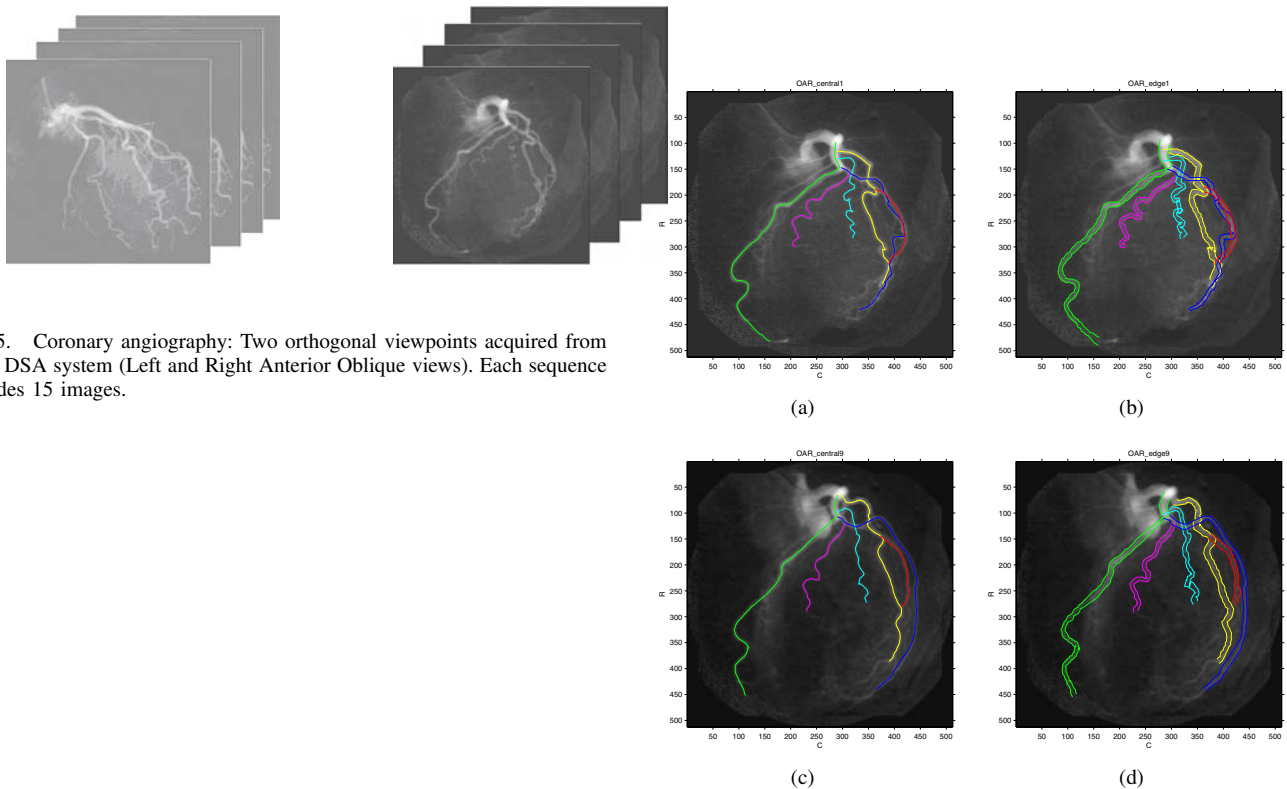


Fig. 7. Extracted centerlines and contours for images 1 and 9 of the RAO sequence

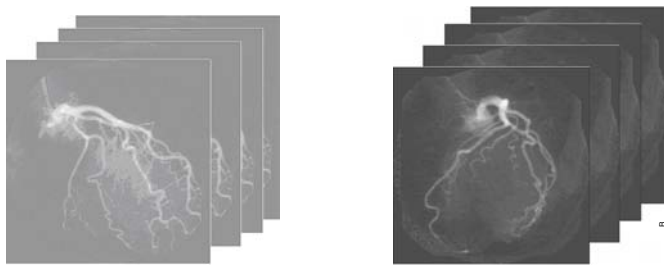


Fig. 5. Coronary angiography: Two orthogonal viewpoints acquired from a GE DSA system (Left and Right Anterior Oblique views). Each sequence includes 15 images.